Improved Reproducibility of PbS Colloidal Quantum Dots Solar Cells Using Atomic Layer–Deposited TiO2

Sukharevska, Nataliia; Bederak, Dmytro; Dirin, Dmitry; Kovalenko, Maksym; Loi, Maria Antonietta

Published in:
Energy Technology

DOI:
10.1002/ente.201900887

Energy Technology
Generation, Conversion, Storage, Distribution
www.entechnol.de

Improved Reproducibility of PbS Colloidal Quantum Dots Solar Cells Using Atomic Layer–Deposited TiO_2

*Nataliia Sukharevska, Dmytro Bederak, Dmitry Dirin, Maksym Kovalenko, and Maria Antonietta Loi**

Thanks to their broadly tunable bandgap and strong absorption, colloidal lead chalcogenide quantum dots (QDs) are highly appealing as solution-processable active layers for third-generation solar cells. However, the modest reproducibility of this kind of solar cell is a pertinent issue, which inhibits the exploitation of this material class in optoelectronics. This issue is not necessarily imputable to the active layer but may originate from different constituents of the device structure. Herein, the deposition of TiO_2 electron transport layer is focused on. Atomic layer deposition (ALD) greatly improves the reproducibility of PbS QD solar cells compared with the previously optimized sol–gel (SG) approach. Power conversion efficiency (PCE) of the solar cells using atomic layer–deposited TiO_2 lies in the range between 5.5% and 7.2%, whereas solar cells with SG TiO_2 have PCE ranging from 0.5% to 6.9% with a large portion of short-circuited devices. Investigations of TiO_2 layers by atomic force microscopy and scanning electron microscopy reveal that these films have very different surface morphologies. Whereas the TiO_2 films prepared by SG synthesis and deposited by spin coating are very smooth, TiO_2 films made by ALD repeat the surface texture of the fluorine-doped tin oxide (FTO) substrate underneath.

1. Introduction

During the past few years, lead chalcogenide (PbS, PbSe) quantum dots (QDs) have been used for various electronic and optoelectronic devices,[1,2] such as transistors,[3] photodetectors,[4] light-emitting diodes,[5] light-emitting field effect transistors,[6] and inverters.[7] They are also among the best materials for implementation in solution-processable solar cells.[8–11] Due to their strong degree of charge-carrier confinement,[12] these QDs provide energy bandgap tunability at the opposite of other solution-processable semiconductors such as organic semiconductors and perovskites, as the bandgap of lead chalcogenides can be also adjusted in the near-infrared (NIR) energy region. This gives us an opportunity to utilize the infrared photons which contribute more than 20% to the total solar spectrum energy. Thus, the use of lead chalcogenide QDs in conjunction with other wider bandgap semiconductors in multiple junction solar cells[13–16] could be a viable strategy to capture the low-energy tail of the solar spectrum. Another important feature of these materials is their large electronic tailorability, in addition to the size tunability. Due to their dimensions, a significant portion of the total number of atoms is located on the surface of the crystals; consequently, their surface has a huge influence on the physical properties. Therefore, the electronic properties can be manipulated by surface modification using various ligands, which allows the alteration of the energy levels as well as concentration and mobility of charge carriers.[17–22] Furthermore, several groups have argued that lead chalcogenide QDs exhibit multiple exciton generation (MEG).[23,24] This phenomenon may help to beat the theoretical limit of efficiency for single junction solar cells.[25] Finally, in comparison with other solution-processable solar cells such as those using organic–inorganic hybrid halide perovskites and conjugated polymers as active layer, PbS QD solar cells are in most cases more robust and less susceptible to oxygen and moisture.[26–28]

Lead chalcogenide QD solar cells have been greatly improved in the past 10 years from the first Schottky-type devices with a power conversion efficiency (PCE) of only a few percent[29–31] to the record certified PCE of 12% in 2018.[32] This large improvement became possible due to several key steps: 1) the progressive development of QD synthesis with the achievement of remarkable monodispersity and control of the QD size and shape[33,34]; 2) the introduction of different passivation strategies to minimize the number of surface traps[35–37] and to achieve higher stability[38]; and 3) the engineering of the solar cell structure.[26,35,39] One of the important milestones toward the development of

N. Sukharevska, D. Bederak, Prof. M. A. Loi
Photophysics & OptoElectronics
Zernike Institute for Advanced Materials
Nijenborgh 4, Groningen, AG 9747, The Netherlands
E-mail: m.a.loi@rug.nl

Dr. D. Dirin, Prof. M. Kovalenko
Department of Chemistry and Applied Biosciences
ETH Zurich
Vladimir Prelog Weg 1, Zurich 8093, Switzerland

The ORCID identification number(s) for the author(s) of this article can be found under https://doi.org/10.1002/ente.201900887.

DOI: 10.1002/ente.201900887

efficient PbS QD solar cells was the introduction of a wide bandgap, n-type metal oxide as an electron transporting layer (ETL) between the transparent conductive oxide (TCO) cathode and the QDs active layer.[39–42] The most studied ETL materials are ZnO and TiO_2, which offer many advantages in terms of energy levels, conductivity, transparency, stability, and processability. Among these two oxides, TiO_2 shows superior chemical and ambient stability.[43] Although there have been many successes, one of the major challenges, namely, the poor reproducibility of QD solar cells from laboratory to laboratory and even from one experiment to another, has yet to be addressed and solved.

The commonly used method for deposition of TiO_2 films is sol–gel (SG) synthesis followed by spin coating and annealing at temperatures above 400 °C.[43–45] This technique is extremely sensitive to small variations in the preparation method, making the supposedly identical films deposited in different research groups hard to compare. Temperature, air humidity, the order of the precursor addition, and the rate of heating used to reach the annealing temperature can all influence the properties of resulting films.[46] The SG oxide deposition may also hinder the realization of the full potential of QD solar cells; for example, a high annealing temperature (450–500 °C) is not compatible with flexible plastic substrates. All the aforementioned factors show that SG synthesis is hindering the technological exploitation of QD solar cells.

In this article, we propose the use of atomic layer deposition (ALD) as an alternative technique for the deposition of the electron extracting layer. This is an industrially scalable technique and has many benefits, such as: 1) atomic control of the thickness; 2) high reproducibility and reliability; 3) large surface area coverage; 4) much lower process temperature; and 5) ability to cover conformally different textured and structured surfaces in contrast to the spin-coating and evaporation techniques. Although ALD has been successfully used for hybrid perovskite and organic semiconductors solar cells,[47–50] very little has been done in QD solar cells.[51,52] In particular, there have been no systematic studies on the comparison between SG- and atomic layer–deposited ETLs in QD solar cells.

Here we report on the performance of PbS QD solar cells incorporating compact TiO_2 ETLs deposited by either SG or ALD. Although similar maximum PCEs could be obtained, the experimental spread of device efficiencies is greatly reduced for solar cells using atomic layer–deposited TiO_2 compared with the one using SG TiO_2. The PCEs of the solar cells fabricated using atomic layer–deposited TiO_2 are found in the narrow range between 5.5% and 7.2%, whereas the solar cells using SG TiO_2 demonstrated a far broader spread of efficiencies between 0.5% and 6.9% with a large number of short-circuited devices. Morphological investigations of the two types of TiO_2 films reveal two very different surfaces, with the atomic layer–deposited sample showing reliable and conformal coating and the SG TiO_2 often displaying pinholes, which presumably are the major reasons for the occurrence of short-circuited devices and for the low device reproducibility. It is also important to underline that the ALD of the TiO_2 ETL was performed at a substantially lower temperature (260 °C) than was used for the SG TiO_2 (450 °C).

2. Results and Discussion

Most of the reported highest efficiency lead chalcogenide QD solar cells are based on the structure, which involves a wide bandgap n-type semiconductor electron transport layer such as ZnO or TiO_2 between the transparent cathode and the QD film.[26,32,45]

For this study, we used the same solar cell structure as described in our recent work,[20] which is shown in **Figure 1**a. It is composed of a TiO_2 ETL deposited on an fluorine-doped tin oxide (FTO) cathode, the pn-homojunction between two adjacent QD layers (QDs treated with tetrabutylammonium chloride (TBAC) for the p-type layer and tetrabutylammonium iodide (TBAI) for the n-type one), a MoO_3 hole transporting layer (HTL), and an Au back contact. The active layer was produced via a layer-by-layer (LBL) method, using oleate-capped PbS QDs with the first excitonic peak in the absorption spectrum at 827 nm (Figure S1, Supporting Information). The completeness of the ligand exchange was verified using Fourier transform infrared (FTIR) spectroscopy measurements (Figure S2, Supporting Information).

The schematic energy band diagram of QD solar cells is shown in Figure 1b. The interface, which is formed between the QD active layer and the TiO_2/FTO cathode, is important for the achievement of high efficiency. TiO_2 simultaneously performs several functions in QD solar cells: 1) it serves as an ETL; 2) it improves selectivity of the cathode by creation of an energy barrier for holes, thus working as a hole-blocking layer (HBL); 3) it limits the recombination losses at the interface with the QD active layers; and 4) it forms the rectifying junction with the QD layer, which ensures a built-in electric field through the QD film.

Our QD solar cells were fabricated with the two types of TiO_2 ETLs, namely, SG TiO_2 prepared by HCl-catalyzed hydrolysis of titanium butoxide and atomic layer–deposited TiO_2 thermally grown from $TiCl_4$ and H_2O (see the Experimental Section for details).

The representation of the typical TiO_2 SG synthesis from titanium butoxide and the thin film deposition strategy is shown in **Figure 2**a. The reaction starts with the acid-catalyzed hydrolysis of the titanium precursor followed by condensation. In the first stage of the SG process, a sol is formed, when the size of the colloidal particles of TiO_2 is not greater than a few tens of nanometers. Further polymerization of the sol results in a network (gel) formation. The last step in the SG preparation

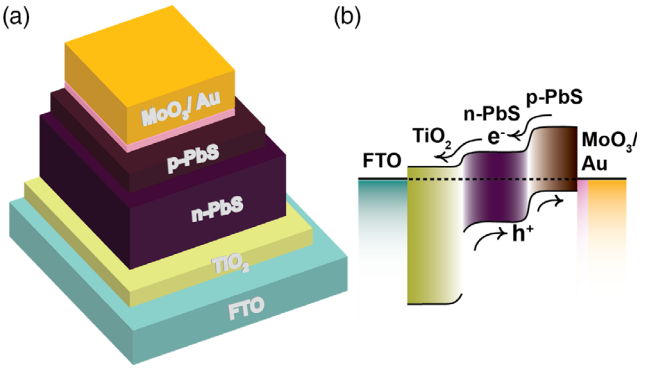

Figure 1. a) Structure of the inverted PbS QD solar cell. b) Energy band diagram of this type of device in dark at open circuit voltage.

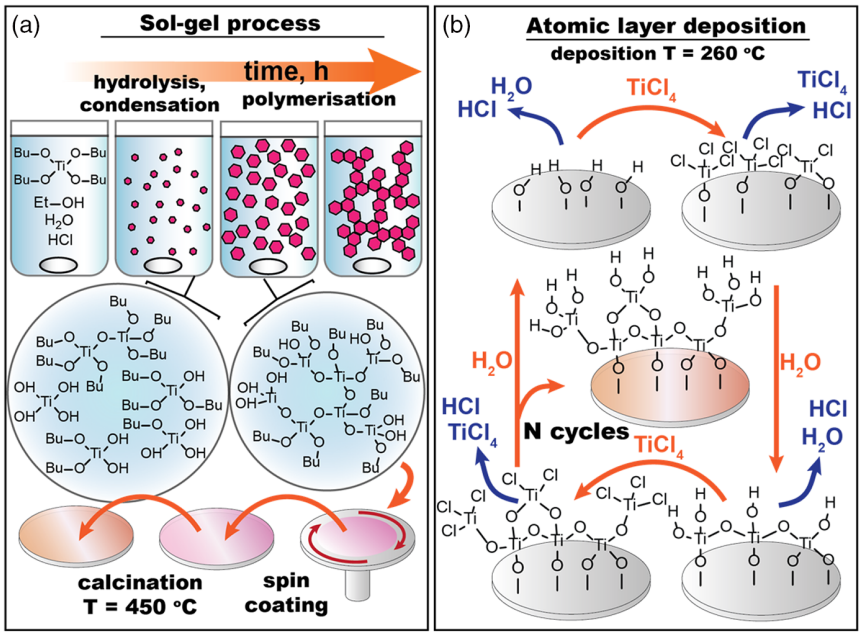

Figure 2. a) SG preparation of the TiO_2. In the first stage, titanium butoxide reacts with water and then the condensation reaction occurs between two hydrolyzed molecules, forming Ti—O—Ti bridges. After multiple condensation events, large polymeric structures are formed. Then the sol is deposited by spin coating and films are annealed for calcinations. b) ALD of the TiO_2 films, which includes alternating reactions of the $TiCl_4$ and H_2O with the surface groups and leads to the formation of a compact TiO_2 layer on the FTO front contact.

of the TiO_2 films is usually gel calcination at a high temperature, to remove solvents and sometimes to improve crystallinity. During the SG preparation of TiO_2, multiple factors may be responsible for variations in the oxide properties; some of them are described in the Supporting Information.

An alternative strategy to deposit TiO_2 thin films is ALD; the main chemical steps of this technique are shown in Figure 2b. TiO_2 films are grown by the sequential pulsing of $TiCl_4$ and H_2O sources separated by a step of purging of the reaction chamber with N_2. This technique is based on two sequential self-limited reactions of the gas precursors with the substrate surface, so the thickness of the oxide film can be easily tuned by changing the number of deposition cycles. It is consequent from the chemical growth mechanism that the atomic layer–deposited layers are very tolerant to the surface topography; i.e., they are conformal for high-aspect ratio structures.

We performed atomic force microscopy (AFM) measurements (**Figure 3**) to study the morphology of the TiO_2 films. The surface

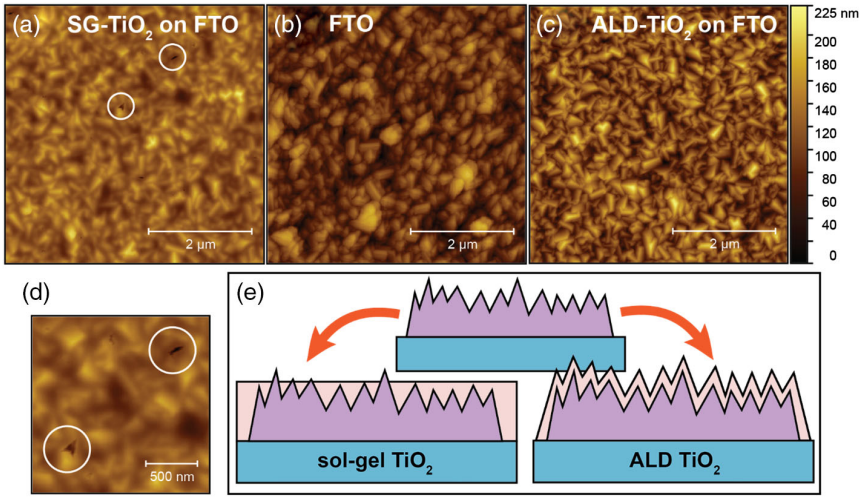

Figure 3. Atomic force micrographs of a) an FTO substrate with TiO_2 deposited by SG spin coating (the white circles underline the presence of deep pinholes), b) a bare FTO substrate, c) an FTO substrate with TiO_2 deposited by 500 cycles of the ALD, d) a magnified view of the micrograph in (a), and e) a schematic of the SG and ALD-covered cathodes explaining the larger amount of shorted devices. The vertical scale is the same for all the AFM micrographs.

of a bare FTO film (Figure 3a) has a relatively high roughness (RMS = 29.4 nm). The FTO substrate with SG TiO_2 displays an RMS of 18.9 nm, whereas the FTO with atomic layer–deposited TiO_2 film had an RMS similar to the bare FTO (29.7 nm). SG-deposited films were much smoother than atomic layer–deposited films and bare FTO substrates. Similar morphological results were obtained from the surface study by scanning electron microscopy (SEM), as shown in Figure S7, Supporting Information. On the AFM images, SG TiO_2 displays pinholes within the films, which may be one of the reasons for a larger portion of shorted and low-performing devices when using SG TiO_2. Spin coating of a sol on top of the rough surface of FTO does not always cover the highest peaks, which may become the reason for the large number of shorted devices. Similar explanations of the device's leakage have been provided in the work of Chen and coworkers,[53] where the authors show that the TiO_2 layer formed by spin coating on top of FTO is highly irregular with numerous pinholes on the oxide surface.

In contrast to SG, the ALD method shows a high surface tolerance; therefore, any surface feature can be fully covered, reducing the possibility that the two opposite electrodes of the device enter in direct contact. Our results of morphological investigations of atomic layer–deposited TiO_2 are in line with the literature reports. For example, atomic layer–deposited TiO_2 has been used for vapor-grown $MAPbI_{3-x}Cl_x$ planar perovskite solar cells and compared with conventional TiO_2 deposited by spin coating.[54] In this study, SEM images where an ultrathin atomic layer–deposited TiO_2 uniformly covers the FTO substrate following the texture of it while spin-coated TiO_2 makes a smooth layer, leaving the FTO spikes exposed, were shown.

Figure 4a shows the performance of the best PbS QD solar cells fabricated with different TiO_2 ETLs, measured under solar-simulated AM1.5G illumination at the intensity of 1000 W m^{-2}.

The device fabricated on an SG TiO_2 ETL shows a short circuit current density (J_{SC}) of 25.0 mA cm^{-2}, an open circuit voltage (V_{OC}) of 0.53 V, and a fill factor (FF) of 52%, resulting in a PCE of 6.9%. The performance of the PbS QD solar cell with atomic layer–deposited TiO_2 ETL is very similar to that of the device with SG TiO_2: a J_{SC} of 24.1 mA cm^{-2}, a V_{OC} of 0.54 V, an FF of 55%, and a PCE of 7.2%. The small differences in FF and J_{SC} of these two champion devices may be explained by the light soaking effect, which is discussed later in this work. **Table 1** shows the performance of the aforementioned solar cells in both forward and reverse scanning modes.

The plots of the *J–V* measurements in the dark for the two types of solar cells are shown in the insert of Figure 4a. This figure shows that these two particular devices perform well as diodes, and both are able to provide a good current rectification: the rectification ratios $\left(\frac{J_{V=2}}{J_{V=-2}}\right)$ are 1.2×10^3 and 9.8×10^2 for the device using SG TiO_2 and atomic layer–deposited TiO_2, respectively. High rectification ratio means lower current leakage, which decreases the shunt resistance of the devices.

External quantum efficiency (EQE) spectra of the two record devices are shown in Figure 4b. They have a similar shape and the same position of the first excitonic peak. The EQE maximum is about 90% in the high-energy region for both devices, which is an indication of efficient conversion of the high-energy photons to electron–hole pairs. In the low-energy region, the EQE of the solar cell using SG TiO_2 is slightly higher than one of the devices fabricated with atomic layer–deposited TiO_2. A possible explanation of this difference may be again the light soaking; in fact, both devices tend to improve after some time under illumination; thus, the EQE spectra slightly vary depending on the previous treatment of the device. The values of the J_{SC} obtained from the integration of the EQE spectra are in good agreement with the J_{SC} values from the *J–V* measurements (23.7 mA cm^{-2} for

Table 1. Figures of merit in forward and reverse sweeps of PbS QD solar cells using SG TiO_2 and atomic layer–deposited TiO_2.

	TiO_2 by SG method		TiO_2 by ALD (500 cycles)	
	Forward sweep	Reverse sweep	Forward sweep	Reverse sweep
J_{SC} [mA cm^{-2}]	25.3	25.0	24.3	24.1
V_{OC} [V]	0.54	0.53	0.56	0.54
FF [%]	50	52	51	55
PCE [%]	6.8	6.9	6.9	7.2

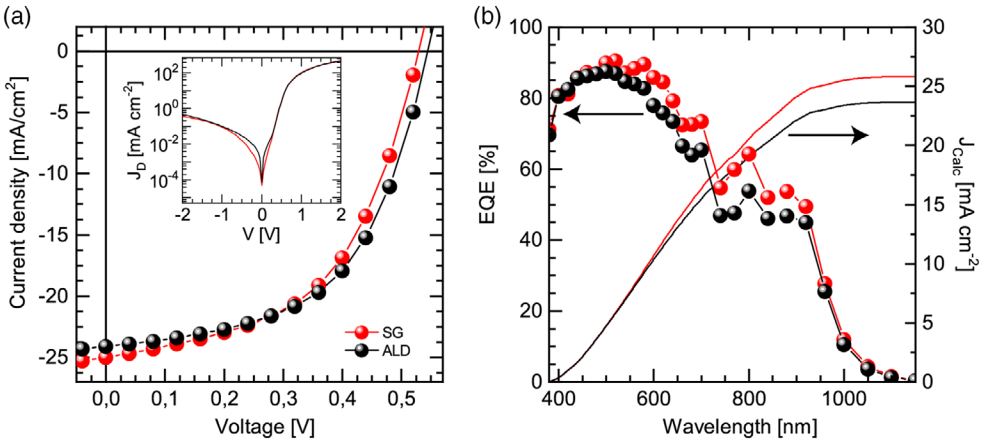

Figure 4. a) *J–V* measurements of PbS QD solar cells with TiO_2 ETL prepared by SG synthesis (red curve) and by ALD (black curve); the insert shows *J–V* measurements of the same devices in the dark. b) Comparison of EQE spectra of the same devices as in (a).

the device fabricated with atomic layer–deposited TiO_2 and 25.9 mA cm^{-2} for the device using SG TiO_2).

The light soaking phenomena have been already observed and discussed for PbS QD solar cells.[55] However, it is mostly reported that the device performance gradually decreases over time under light exposure mostly due to the decrease in J_{SC}. **Figure 5**a shows a comparison of the first *J–V* measurements of fresh devices with both types of ETL and the measurements of the same devices after a period of light soaking. Figure 5b shows the behavior of the same devices before and after light soaking after a night of storage in the nitrogen atmosphere. The evolution for 25 min of the solar cell parameters of both devices is shown in Figure 5c,d.

The first *J–V* measurements of both devices have large current density hysteresis for the forward and reverse scans and low values of J_{SC} (around 21 mA cm^{-2} for both). The solar cell with atomic layer–deposited TiO_2 also shows an s-shape in forward sweep at the first light exposure, which can be an indication of an energy barrier, and of the insufficient conductivity of the atomic layer–deposited TiO_2 before illumination. We indeed observed an improvement of the conductivity of atomic layer–deposited TiO_2 after light exposure (Figure S3, Supporting Information). The sheet resistance of atomic layer–deposited TiO_2 in the dark is measured to be 7.67E+11 Ω, whereas the one of SG TiO_2 is higher and did not give a measurable value.

As mentioned earlier, a possible explanation for the s-shape in the *J–V* curve is an energy barrier at the interface between the oxide and QD layer. Exposure to light improves the performance of the devices, especially on the first day, mostly due to increases in the J_{SC} and the FF and a reduction of the hysteresis. The s-shape of the *J–V* curves of the device with atomic layer–deposited TiO_2 continuously decreased during illumination and almost

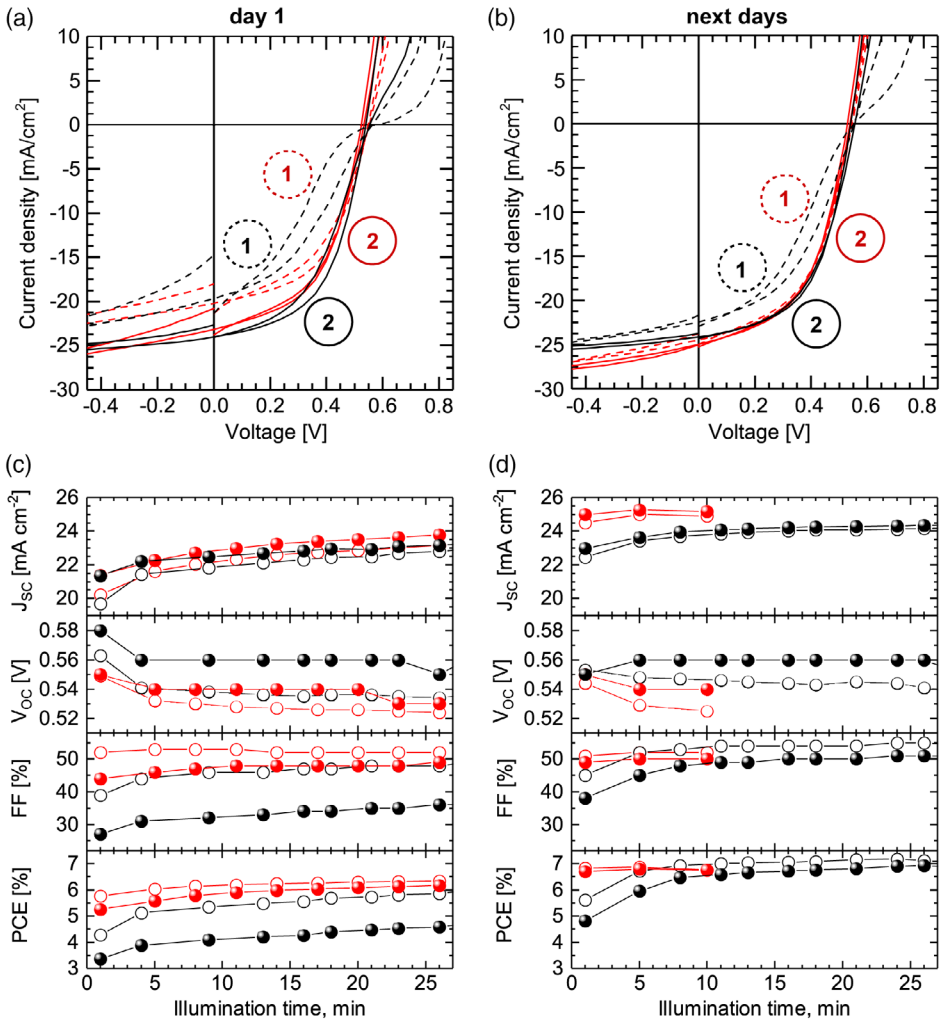

Figure 5. Behavior of PbS QD solar cells using TiO_2 ETL prepared by SG method (red line) and ALD (black line) under continuous illumination. a) The first *J–V* measurement is shown by a dashed line, and the solid lines are the *J–V* measurements when the parameters have reached saturation. b) The same measurements on the same devices as in (a) after one-day storage in the glove box. c) Evolution of the device parameters during the light soaking time on the first day. d) Evolution of the device parameters during the light soaking time on the second day. Black color indicates the device using atomic layer–deposited TiO_2 ETL, and the red color indicates the ones using SG TiO_2. Device parameters determined from the forward scans are indicated by filled circles, whereas the ones from reverse scans are indicated by empty circles.

disappeared after around 40 min, whereas the FF increases from around 38% to 48%. At the opposite end, the FF of the devices using SG TiO_2 is more constant over the whole illumination period. Figure S4, Supporting Information, shows the evolution of the parameters of the solar cells under longer illumination time. The J_{SC} of both devices increases significantly after illumination; this overall behavior may be interpreted as an indication of the filling of trap states. The V_{OC} of both types of devices decreases within the first 5 min and then remains constant. A similar feature has been previously described for other PbS QD solar cells and is ascribed to the measurement stress effects due to light soaking under open circuit conditions.[56] To summarize, both devices improve because of light soaking, but variations in the atomic layer–deposited TiO_2-based device are more pronounced, and a longer time is necessary to achieve their peak performance (around 100 vs 30–40 min for the devices using SG TiO_2). For both types of devices, performance became stable after the maximum values were achieved. These observations agree with previous literature showing that the level of electron doping in TiO_2 can vary with the illumination.[57]

On the second day and later, both types of devices display overall better performance than on the first day, driven by the improvement in the J_{SC} and the FF (Figure 5b). Furthermore, on the second day of measurements, they both achieved the peak values of performance in a much shorter time of illumination (a few minutes for the device with SG TiO_2 and around 20 min for the device with atomic layer–deposited TiO_2). Also, almost no hysteresis in the J–V measurements and no s-shape was recorded. In between the testing, devices were stored in a nitrogen atmosphere; therefore, any kind of explicit oxidation which often causes initial improvements in the PbS QDs solar cells due to the increase in doping of the p-type PbS QDs layer is excluded. At this point, performances saturated, and the device did not change for up to 80 days.

These results demonstrate that ETL grown by ALD can be inserted in the QD solar cell device structure without losing in device performance. Moreover, the deposition of 500 cycles of atomic layer–deposited TiO_2 (around 20 nm) is enough to obtain the same performance as the best devices with SG TiO_2 (28 nm). It is important to underline that although these solar cells show parameters very similar to those obtained with SG TiO_2, the experimental variation of the device performance is extremely different (**Figure 6**). Devices without any ETL show much lower performance, with low V_{OC}, J_{SC}, FF, and a huge number of short-circuited devices, as was expected. Devices with very thin atomic layer–deposited TiO_2 (150–300 ALD cycles) show much better V_{OC} and FF (Figure 6) than the devices without ETL but generally result in a larger spread in their parameters, which is probably due to the limited blocking activity toward holes of this very thin layer. Further increase in the thickness of atomic layer–deposited TiO_2 from 500 to 1000 cycles allows a better reproducibility of the devices.

Figure 6 shows that the main advantage of the atomic layer–deposited TiO_2 films with respect to the SG TiO_2 is the much higher degree of reproducibility of the device performance. Furthermore, all the dark J–V measurements within one substrate (generally four areas) are identical (Figure S5, Supporting Information), with rectification ratio around 1.0E+3, implying the homogeneity of the ALD layers. It is important to note that

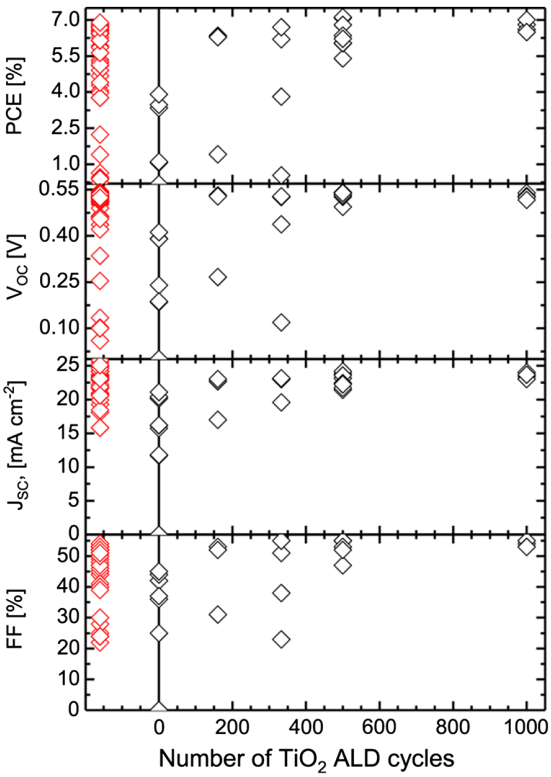

Figure 6. Variation of the device's parameters depending on the TiO_2 deposition and thickness. The red symbols correspond to devices fabricated with SG TiO_2, and the black symbols are related to devices fabricated with atomic layer–deposited TiO_2 prepared by different numbers of ALD cycles.

the experimental variation becomes the smallest when more than 500 ALD cycles are used. Shorted devices were never observed when using an optimal thickness of atomic layer–deposited TiO_2, whereas several shorted pixels are often observed for devices with SG TiO_2. The best figures of merits as well as the average values and the standard deviations of devices with SG TiO_2, with different thicknesses of atomic layer–deposited TiO_2 and without TiO_2, can be found in Table S1, Supporting Information.

Finally, the deposition of a thin layer of atomic layer–deposited TiO_2 on the top of SG TiO_2 was tested in solar cells as a strategy to passivate the SG oxide. This resulted in well-performing devices (Figure S6, Supporting Information) without short-circuited areas. The parameters of devices fabricated on a combined SG and atomic layer–deposited TiO_2 layer are shown in Table S2, Supporting Information. Thus, ALD can also be used as one of the approaches to improve the quality of the oxide layer deposited with cheaper techniques.

3. Conclusions

In summary, we replaced the widely used SG method of preparing TiO_2 layer in PbS QD solar cells with the ALD method. ALD is an industrially scalable technique which can be used for

pinholes-free ETL deposition, which becomes more essential when going from prototypes to real large area solar cell modules. By optimizing the thickness of the atomic layer–deposited TiO_2, we obtained devices with very similar performance (about 7%) to that of the best devices fabricated with SG TiO_2. Importantly, the atomic layer–deposited TiO_2-based devices showed a much higher reproducibility and lower variation in performance. Morphological study indicated that atomic layer–deposited TiO_2 covers all the surface features, whereas SG TiO_2 smoothens the FTO surface, leaving spikes and imperfections such as pinholes that give rise to shorted devices.

Furthermore, the atomic layer–deposited TiO_2 is deposited at 260 °C, which is a much lower temperature than the one used for the SG TiO_2 (450–500 °C). This allows the use of different types of substrates. A further lowering of the deposition temperature might enable us to invert the solar cell structure and to deposit the TiO_2 on top of PbS QDs films. Finally, doping could be used to reduce the energy barrier and the s-shape of the *J–V* curves, which has a detrimental effect on the FF and on the overall device performance.

4. Experimental Section

Lead Sulfide Colloidal Quantum Dot Synthesis: Lead sulfide colloidal quantum dots (PbS CQDs) capped with oleate ligands were synthesized by the hot injection method. As a lead precursor, lead (II) acetate trihydrate ($PbAc_2{\cdot}3H_2O$) was used (1.516 g). $PbAc_2{\cdot}3H_2O$ powder was mixed with octadecene (ODE, 47.5 mL) and oleic acid (OA, 2.5 mL). Then the lead precursor solution was dried for 1 h under vacuum at 120 °C in a three-neck reaction flask, using a Schlenk line. As a sulfur precursor, bis(trimethylsilyl) sulfide (TMS_2S) was used. TMS_2S (0.420 mL) was dissolved in dried ODE (10 mL) in the nitrogen-filled glovebox. The reaction was conducted under a nitrogen atmosphere. The lead precursor solution was heated to 90 °C, and when the temperature reached this point, the heating mantle was removed, and the sulfur precursor solution was quickly injected to the lead precursor solution. After 1 min of QD growth, OA (3 mL) was injected, and the reaction was quenched by cooling the reaction flask down to room temperature, using a cold-water bath. To isolate the nanocrystals, hexane (30 mL) and ethanol (144 mL) were added, followed by centrifugation. CQDs were redispersed in hexane and precipitated by minimum amount of ethanol two more times. Finally, PbS CQDs were redispersed in hexane. Solution concentrations were determined by the measurement of the absorption of diluted solutions at 400 nm. For the following building of the devices, the solution of PbS QDs with a first excitonic peak in the absorption spectrum at 827 nm was used. Thus, the bandgap value was 1.5 eV, and the nanocrystal size was about 2.6 nm.

Device Fabrication: Prepatterned glass substrates with fluorine-doped tin oxide SnO_2: F (FTO) (13 $\Omega\,sq^{-1}$), purchased from Visiontek Systems Ltd., were cleaned with detergent and then subsequently sonicated in acetone and isopropanol and dried in an oven at 120 °C for at least 20 min. Then the FTO substrates were treated with UV O_3 to remove any possible organic residues and to improve the wettability of the substrates.

Sol–Gel Method for Preparation of TiO_2 Films: Titanium oxide sol was prepared by mixing ethanol, titanium (IV) butoxide, and HCl (37%) in the v/v ratio 20:2:1. Then the sol was stirred for at least 30 min and spin cast onto FTO substrates. Thus, the gel was formed after solvent removal.[45] Substrates with TiO_2 gel were annealed by raising the temperature from room temperature to 450 °C for 30 min. The substrates were slowly cooled down from 450 °C to room temperature to avoid crack formation due to abrupt changes of temperature.

Atomic Layer Deposition of TiO_2 Films: Before deposition, the substrates were left in the vacuum chamber for 20 min at the deposition temperature for the stabilization. The TiO_2 HBL was deposited at 260 °C from $TiCl_4$ (0.1 s pulse, 4 s purging time, 150 sccm N_2 flow) and H_2O (0.1 s pulse, 6 s purging time, 200 sccm N_2 flow).

PbS Quantum Dot Solar Cell Fabrication: PbS CQD films were fabricated in a nitrogen-filled glove box by an LBL spin-casting method. Oleate-capped PbS QDs were spin cast from hexane solutions (10 mg mL^{-1}) onto the earlier prepared TiO_2 films. Ligand exchange was performed by subjecting the films to the 15 mg mL^{-1} methanol solution of TBAI or TBAC for 30 s. To get rid of the products of the ligand exchange and the excess of unreacted ligands after the ligand exchange, the films were washed twice with methanol. The cycles of deposition of the hexane solution of PbS QDs, the ligand exchange, and the washing were repeated 12 times for TBAI-treated layers and 4 times for TBAC-treated layers to reach the total thickness of the QD active layer of about 280 nm. In total, 44 devices with SG TiO_2, 8 without ETL, and 20 with atomic layer–deposited TiO_2, of which 4 with 160 cycles, 4 with 333 cycles, 8 with 500 cycles, and 4 with 1000 cycles, were fabricated.

Back Electrode Deposition: The devices were finalized by thermal evaporation of 5 nm MoO_3 and 80 nm gold under the pressure of 5×10^{-8} mBar at the rates of 0.2 and 0.5–2 Å s^{-1}, respectively. The device area defined by the overlap of FTO and Au electrodes was 0.16 cm^2. After Au deposition, *J–V* characteristics of the devices were measured for the first time, and next the devices were kept in a nitrogen-filled glovebox.

Current–Voltage Characterization: *J–V* measurements were conducted in a nitrogen-filled glove box under simulated AM1.5G solar illumination, using a Steuernagel Solar constant 1200 metal halide lamp set to 100 mW cm^{-2} intensity and a Keithley 2400 SourceMeter. Light was calibrated using a monocrystalline silicon solar cell (WRVS reference cell, Fraunhofer ISE) and corrected for the spectral mismatch. For efficiency calculations, the illuminated area was confined by the shadow mask (0.10 cm^2) to avoid any edge effects. The temperature was set to 295 K by a flux of cold N_2.

The External Quantum Efficiency Measurements: The EQE was measured under monochromatic light at short circuit conditions. For the source of white light, a 250 W quartz tungsten halogen lamp (6334NS, Newport) with lamp housing (67009, Newport) was used. Narrow bandpass filters (Thorlabs) with a full width half maximum (FWHM) of 10 ± 2 nm from 400 to 1300 nm and an FWHM of 12 ± 2.4 nm from 1300 to 1400 nm were used for monochromatic light. The light intensity was determined by calibrated PD300 and PD300IR photodiodes (Ophir Optics) for the visible and infrared parts of the spectrum, respectively.

Morphological Characterization: AFM measurements were obtained under ambient conditions. The AFM images were taken with a Bruker microscope (MultiMode 8 with ScanAsyst) in ScanAsyst Peak Force Tapping mode with SCANASYST-AIR probes having elastic constant $k = 0.4$ N m^{-1}, a resonance frequency of 70 kHz, and a tip radius less than 12 nm (nominal 2 nm). The images were taken with a scan rate of 0.98 Hz and the resolution of 1024 lines/sample. The SEM images were obtained using the FEI Nova Nano SEM 650.

Thickness Measurements: The thicknesses of the PbS CQD films were measured by a profilometer (Dektak 6M Stylus Profiler Veeco). The thickness of TiO_2 was controlled by ellipsometry and X-ray reflectivity.

Supporting Information

Supporting Information is available from the Wiley Online Library or from the author.

Acknowledgements

N.V.S. and M.A.L. acknowledge the financial support of the ERC Starting Grant "Hybrids Solution Processable Optoelectronic Devices" (Hy-SPOD) (ERC306983). Teodor Zaharia is acknowledged for help with ellipsometry measurements, Gert ten Brink is acknowledged for assistance with SEM imaging, and Arjen Kamp is acknowledged for the technical support.

Conflict of Interest

The authors declare no conflict of interest.

Keywords

atomic layer deposition, electron transporting layers, quantum dots, solar cells, titanium dioxide

Received: July 23, 2019
Revised: October 2, 2019
Published online: October 28, 2019

[1] D. M. Balazs, M. A. Loi, *Adv. Mater.* **2018**, *30*, 1800082.
[2] J. Y. Kim, O. Voznyy, D. Zhitomirsky, E. H. Sargent, *Adv. Mater.* **2013**, *25*, 4986.
[3] D. M. Balazs, N. Rizkia, H. H. Fang, D. N. Dirin, J. Momand, B. J. Kooi, M. V. Kovalenko, M. A. Loi, *ACS Appl. Mater. Interfaces* **2018**, *10*, 5626.
[4] A. De Iacovo, C. Venettacci, L. Colace, L. Scopa, S. Foglia, *Sci. Rep.* **2016**, *6*, 1.
[5] S. Pradhan, F. Di Stasio, Y. Bi, S. Gupta, S. Christodoulou, A. Stavrinadis, G. Konstantatos, *Nat. Nanotechnol.* **2019**, *14*, 72.
[6] A. G. Shulga, S. Kahmann, D. N. Dirin, A. Graf, J. Zaumseil, M. V. Kovalenko, M. A. Loi, *ACS Nano* **2018**, *12*, 12805.
[7] A. G. Shulga, V. Derenskyi, J. M. Salazar-Rios, D. N. Dirin, M. Fritsch, M. V. Kovalenko, U. Scherf, M. A. Loi, *Adv. Mater.* **2017**, *29*, 1701764.
[8] Z. Liu, J. Yuan, S. A. Hawks, G. Shi, S. Lee, W. Ma, *Sol. RRL* **2017**, *1*, 1600021.
[9] G. H. Carey, A. L. Abdelhady, Z. Ning, S. M. Thon, O. M. Bakr, E. H. Sargent, *Chem. Rev.* **2015**, *115*, 12732.
[10] V. Malgras, A. Nattestad, J. H. Kim, S. X. Dou, Y. Yamauchi, *Sci. Technol. Adv. Mater.* **2017**, *18*, 334.
[11] O. E. Semonin, J. M. Luther, M. C. Beard, *Mater. Today* **2012**, *15*, 508.
[12] F. W. Wise, *Acc. Chem. Res.* **2000**, *33*, 773.
[13] R. W. Crisp, G. F. Pach, J. M. Kurley, R. M. France, M. O. Reese, S. U. Nanayakkara, B. A. Macleod, D. V. Talapin, M. C. Beard, J. M. Luther, *Nano Lett.* **2017**, *17*, 1020.
[14] Y. Bi, S. Pradhan, M. Z. Akgul, S. Gupta, A. Stavrinadis, J. Wang, G. Konstantatos, *ACS Energy Lett.* **2018**, *3*, 1753.
[15] X. Wang, G. I. Koleilat, J. Tang, H. Liu, I. J. Kramer, R. Debnath, L. Brzozowski, D. A. R. Barkhouse, L. Levina, S. Hoogland, E. H. Sargent, *Nat. Photonics* **2011**, *5*, 480.
[16] G. Shi, Y. Wang, Z. Liu, L. Han, J. Liu, Y. Wang, K. Lu, S. Chen, X. Ling, Y. Li, S. Cheng, W. Ma, *Adv. Energy Mater.* **2017**, *7*, 1602667.
[17] S. J. Oh, N. E. Berry, J. H. Choi, E. A. Gaulding, T. Paik, S. H. Hong, C. B. Murray, C. R. Kagan, *ACS Nano* **2013**, *7*, 2413.
[18] P. R. Brown, D. Kim, R. R. Lunt, N. Zhao, M. G. Bawendi, J. C. Grossman, V. Bulović, *ACS Nano* **2014**, *8*, 5863.
[19] D. F. Garcia-Gutierrez, L. P. Hernandez-Casillas, M. V. Cappellari, F. Fungo, E. Martínez-Guerra, D. I. García-Gutiérrez, *ACS Omega* **2017**, *3*, 393.
[20] D. Bederak, D. M. Balazs, N. V. Sukharevska, A. G. Shulga, M. Abdu-Aguye, D. N. Dirin, M. V. Kovalenko, M. A. Loi, *ACS Appl. Nano Mater.* **2018**, *1*, 6882.
[21] L. Liu, S. Z. Bisri, Y. Ishida, D. Hashizume, T. Aida, Y. Iwasa, *ACS Appl. Nano Mater.* **2018**, *1*, 5217.
[22] R. D. Harris, S. Bettis Homan, M. Kodaimati, C. He, A. B. Nepomnyashchii, N. K. Swenson, S. Lian, R. Calzada, E. A. Weiss, *Chem. Rev.* **2016**, *116*, 12865.
[23] O. E. Semonin, J. M. Luther, S. Choi, H.-Y. Chen, J. Gao, A. J. Nozik, M. C. Beard, *Science* **2011**, *334*, 1530.
[24] A. J. Nozik, M. C. Beard, J. M. Luther, M. Law, R. J. Ellingson, J. C. Johnson, *Chem. Rev.* **2010**, *110*, 6873.
[25] W. Shockley, H. J. Queisser, *J. Appl. Phys.* **1961**, *32*, 510.
[26] C.-H. M. Chuang, P. R. Brown, V. Bulović, M. G. Bawendi, *Nat. Mater.* **2014**, *13*, 796.
[27] Z. Ning, O. Voznyy, J. Pan, S. Hoogland, V. Adinolfi, J. Xu, M. Li, A. R. Kirmani, J. Sun, J. Minor, K. W. Kemp, H. Dong, L. Rollny, A. Labelle, G. Carey, B. Sutherland, I. Hill, A. Amassian, H. Liu, J. Tang, O. M. Bakr, E. H. Sargent, *Nat. Mater.* **2014**, *13*, 4.
[28] J. M. Salazar-Rios, N. Sukharevska, M. J. Speirs, S. Jung, D. Dirin, R. M. Dragoman, S. Allard, M. V. Kovalenko, U. Scherf, M. A. Loi, *Adv. Mater. Interfaces* **2018**, *5*, 1801155.
[29] K. W. Johnston, A. G. Pattantyus-Abraham, J. P. Clifford, S. H. Myrskog, D. D. MacNeil, L. Levina, E. H. Sargent, *Appl. Phys. Lett.* **2008**, *92*, 90.
[30] J. M. Luther, M. Law, M. C. Beard, Q. Song, M. O. Reese, R. J. Ellingson, A. J. Nozik, *Nano Lett.* **2008**, *8*, 3488.
[31] C. Piliego, L. Protesescu, S. Z. Bisri, M. V. Kovalenko, M. A. Loi, *Energy Environ. Sci.* **2013**, *6*, 3054.
[32] J. Xu, et al., *Nat. Nanotechnol.* **2018**, *13*, 456.
[33] Z. Huang, G. Zhai, Z. Zhang, C. Zhang, Y. Xia, L. Lian, X. Fu, D. Zhang, J. Zhang, *CrystEngComm* **2017**, *19*, 946.
[34] X. Yao, Z. Song, L. Mi, G. Li, X. X. Wang, X. X. Wang, Y. Jiang, *Sol. Energy Mater. Sol. Cells* **2017**, *164*, 122.
[35] S. Pradhan, A. Stavrinadis, S. Gupta, S. Christodoulou, G. Konstantatos, *ACS Energy Lett.* **2017**, *2*, 1444.
[36] A. H. Ip, S. M. Thon, S. Hoogland, O. Voznyy, D. Zhitomirsky, R. Debnath, L. Levina, L. R. Rollny, G. H. Carey, A. Fischer, K. W. Kemp, I. J. Kramer, Z. Ning, A. J. Labelle, K. W. Chou, A. Amassian, E. H. Sargent, *Nat. Nanotechnol.* **2012**, *7*, 577.
[37] X. Lan, O. Voznyy, A. Kiani, F. P. García de Arquer, A. S. Abbas, G.-H. Kim, M. Liu, Z. Yang, G. Walters, J. Xu, M. Yuan, Z. Ning, F. Fan, P. Kanjanaboos, I. Kramer, D. Zhitomirsky, P. Lee, A. Perelgut, S. Hoogland, E. H. Sargent, *Adv. Mater.* **2016**, *28*, 299.
[38] Y. Cao, A. Stavrinadis, T. Lasanta, D. So, G. Konstantatos, *Nat. Energy* **2016**, *1*, 16035.
[39] A. G. Pattantyus-Abraham, I. J. Kramer, A. R. Barkhouse, X. Wang, G. Konstantatos, R. Debnath, L. Levina, I. Raabe, M. K. Nazeeruddin, M. Grätzel, E. H. Sargent, *ACS Nano* **2010**, *4*, 3374.
[40] J. M. Luther, J. Gao, M. T. Lloyd, O. E. Semonin, M. C. Beard, A. J. Nozik, *Adv. Mater.* **2010**, *22*, 3704.
[41] K. S. Leschkies, T. J. Beatty, M. S. Kang, D. J. Norris, E. S. Aydil, *ACS Nano* **2009**, *3*, 3638.
[42] M. J. Choi, S. Kim, H. Lim, J. Choi, D. M. Sim, S. Yim, B. T. Ahn, J. Y. Kim, Y. S. Jung, *Adv. Mater.* **2016**, *28*, 1780.
[43] R. L. Z. Hoye, K. P. Musselman, J. L. MacManus-Driscoll, *APL Mater.* **2013**, *1*, 060701.
[44] A. Lewkowicz, A. Synak, B. Grobelna, P. Bojarski, R. Bogdanowicz, J. Karczewski, K. Szczodrowski, M. Behrendt, *Opt. Mater.* **2014**, *36*, 1739.
[45] M. J. Speirs, D. N. Dirin, M. Abdu-Aguye, D. M. Balazs, M. V. Kovalenko, M. A. Loi, M. Antonietta, *Energy Environ. Sci.* **2016**, *9*, 2916.
[46] C. J. Brinker, G. W. Scherer, *Sol-Gel Science*, Elsevier, Amsterdam/New York **1990**.
[47] I. S. Kim, R. T. Haasch, D. H. Cao, O. K. Farha, J. T. Hupp, M. G. Kanatzidis, A. B. F. Martinson, *ACS Appl. Mater. Interfaces* **2016**, *8*, 24310.
[48] Y. Wu, X. Yang, H. Chen, K. Zhang, C. Qin, J. Liu, W. Peng, A. Islam, E. Bi, F. Ye, M. Yin, P. Zhang, L. Han, *Appl. Phys. Express* **2014**, *7*, 052301.
[49] E. J. Lee, S. O. Ryu, *J. Electron. Mater.* **2017**, *46*, 961.

[50] V. Zardetto, B. L. Williams, A. Perrotta, F. Di Giacomo, M. A. Verheijen, R. Andriessen, W. M. M. Kessels, M. Creatore, *Sustainable Energy Fuels* **2017**, *1*, 30.
[51] Z. Ning, H. Dong, Q. Zhang, O. Voznyy, E. H. Sargent, *ACS Nano* **2014**, *8*, 10321.
[52] P. Maraghechi, A. J. Labelle, A. R. Kirmani, X. Lan, M. M. Adachi, S. M. Thon, S. Hoogland, A. Lee, Z. Ning, A. Fischer, A. Amassian, E. H. Sargent, *ACS Nano* **2013**, *7*, 6111.
[53] H. Ren, X. Zou, J. Cheng, T. Ling, X. Bai, D. Chen, *Coatings* **2018**, *8*, 314.
[54] S. Na, S. Lee, W.-G. Choi, C.-G. Park, S. O. Ryu, T. Moon, *J. Vac. Sci. Technol. A* **2019**, *37*, 010902.
[55] Z. Yang, A. Janmohamed, X. Lan, F. P. García De Arquer, O. Voznyy, E. Yassitepe, G. H. Kim, Z. Ning, X. Gong, R. Comin, E. H. Sargent, *Nano Lett.* **2015**, *15*, 7539.
[56] B. D. Chernomordik, A. R. Marshall, G. F. Pach, J. M. Luther, M. C. Beard, *Chem. Mater.* **2017**, *29*, 189.
[57] A. Brajsa, K. Szaniawska, R. J. Barczyński, L. Murawski, B. Kościelska, A. Vomvas, K. Pomoni, *Opt. Mater.* **2004**, *26*, 151.